Granular Matter (2023) 25:37
https://doi.org/10.1007/s10035-023-01324-z

ORIGINAL PAPER

Numerical investigation on the influence of water content on collapse of granular columns

Xihua Chu[1] · **Zijian Zhu**[1] · **Lian Wang**[1]

Received: 23 December 2022 / Accepted: 14 March 2023 / Published online: 29 April 2023

Abstract
Water can strongly affect the mechanical behavior of granular materials. In this study, numerical simulation is conducted to investigate the effect of water content described by saturation on the collapse of granular columns. A coupled CFD-DEM model is adopted for the wet granular materials from pendular state to capillary state (saturation from 30 to100%), and the discrete element-liquid bridge model is adopted for the wet granular materials of pendular state (saturation less than 30%). The influence of saturation, particle radius, and friction on the shape of the deposit is studied, and the final deposit boundary is fitted by a bilinear model. In addition, the fluidity is studied by the motion of mass center of granular materials. Numerical examples show that within the saturation range from 0.1 to 0.5% and from 30 to 100%, the water has an obvious effect on final deposit shape. Within the saturation range of 0.5–30%, the water has little effect on the final deposit shape. For the saturation range of 0.1–0.5%, the fluidity decreases with the increase of saturation, and when the saturation is more than 30%, the fluidity increases with the increase of saturation. The study revealed the influence of interstitial water on the fluidity of granular materials, which is significant for the researches of geological engineering problems, such as landslides.

Keywords Wet granular column · Collapse · Liquid-bridge · Fluid-particle coupling · Discrete element method

1 Introduction

Gravity driven wet granular flow, such as debris flow, landslides, and pyroclastic flow, are a common phenomenon and have a significant impact on industrial production and engineering problem. Particles, liquids, and air make up the three phases of the wet granular flow. It is challenging to fully comprehend the behavior of wet granular flow because of its nonlinearity and disorder derived from the complex interactions and motion of particles and interstitial fluid. Contrary to dry granular flow, interstitial water affects wet granular flow significantly. Owing to the liquid surface tension, the cohesion between wet particles should be considered [1]. It is discovered that the capillary force created by the addition of a small amount of liquid significantly affects the flow behavior of granular materials [2]. During the impoundment of the Three Gorges Dam, the infiltration of reservoir water caused the occurrence of Qianjiangping landslide [3], which illustrates interstitial water has an important impact on geological engineering. Therefore, the study of the effect of interstitial water on granular flow is necessary and significant.

The collapse of a granular column is a well-known experiment for studying the behavior of granular flows[4]. Some researchers focus on how interstitial water affects the rate of a particle column collapse. The buoyancy and lubrication force produced by interstitial water decreases the friction between particles, hastening the collapse of the granular column [5]. However, the influence of interstitial water varies with particle radius. Interstitial water accelerates granular column collapse in coarse particles in experiments and numerical simulations of partially submerged granular columns while retarding it in fine particles [6]. In the pendular state, the particle roughness affects the runout distance [7]. More interstitial water is needed for coarse particles to create liquid bridges than that for smooth particles. The other researchers focus on the morphology of collapse flows. The deposition morphology and erosion geometry of a granular column collapse onto an erodible bed was studied by Wu et al. [8]. Through an experiment involving the collapse of saturated and partially saturated granular materials on rigid

✉ Xihua Chu
Chuxh@whu.edu.cn

[1] Department of Engineering Mechanics, School of Civil Engineering, Wuhan University, Wuhan 430072, China

slopes, a new type of discontinuous collapse morphology was discovered [9]. The collapsed states were divided into continuous collapsed and block collapsed based on the flow morphology during the collapse process. The presence of interstitial water has a significant impact on the collapse morphology of the granular column, whereas the variation in water content has a little impact [10]. Through experiments using X-ray tomography, wetting collapse in sand revealed two distinct deformation patterns, vertical shrinkage and isotropic shrinkage [11].

The liquid bridge model and continuum model of interstitial water are primarily used in numerical simulation to simulate the impact of water on granular flow. The liquid bridge model is most frequently employed because of its simplicity, though only a small amount of the liquid volume is applicable [12]. The continuum model based on averaging can more accurately simulate the effect of interstitial water on particles under conditions of high saturation. And the CFD-DEM method has been extensively used in the biological and chemical fields to simulate granular flow under high saturation [13–15]. In this method, the hydrodynamics of the continuum fluid are determined by solving the Navier–Stokes equations based on the concept of local average in the CFD, while the motion information of the discrete particle is obtained by solving Newton's second law through the DEM. The combination of CFD and DEM was first attempted by Tanaka et al. in the simulation of the two-dimensional fluidized bed [16]. Li et al. developed a discrete particle–continuum model for modeling the coupled hydro-mechanical behavior in saturated granular materials [17]. The motion of the interstitial fluid is described by two parallel continuum schemes governed by the averaged incompressible Navier–Stokes equations and Darcy's law, respectively. To increase the computation range of particle size without impacting the precision of the fluid grid, the porous sphere technique was incorporated into the CFD-DEM model [18]. Besides, micropolar fluid model was also adopted to describe the multiphase system with multi-size particles under the coupling with discrete particles [19].

Now, numerical simulation and experimental research on the granular column collapsed typically concentrates the case of low water content [10]. In this study, the collapsed behavior of granular column with various water content from low to fully saturated is investigating, and the water content is described by saturation. By creating uniform initial saturation conditions, the mechanical behavior of wet granular column collapse under various saturations is simulated. The effects of saturation, particle radius, friction coefficient, final deposit shape, and granular column fluidity are studied. The three-phase coupled CFD-DEM model and the liquid bridge model are briefly introduced in the second section. The third section primarily introduces the simulation process and its variables. The numerical simulation is validated by comparison with the experimental data in the fourth section. The dynamics of collapsed states as well as the effects of particle radius, friction coefficient, and saturation on the final deposit shape, are investigated. To study the variation in deposit shape, the bilinear model is used to fit the final deposit boundary. In addition, referring to the method describing the fluidity of dry particles [20], the fluidity of a collapsed granular column was investigated by the mass center motion and angle of mass center motion.

2 Liquid-bridge model and CFD-DEM model

2.1 Discrete particle model and discrete element method

In DEM(discrete element method) [21], the core is the equation of motion of particles and the contact model between particles. The motion of each particle is governed by

$$m_i \frac{dv_i}{dt} = \sum_{j=1}^{k_c} (f_{n,ij} + f_{t,ij}) + m_i g + f_l \tag{1}$$

$$I_i \frac{dw_i}{dt} = \sum_{j=1}^{k_c} (M_{t,ij} + M_{r,ij}) \tag{2}$$

where, $f_{n,ij}$ and $f_{t,ij}$ are respectively the normal contact force and tangential contact force between particles i and j. The f_l is the particle–fluid interaction force acting on the particle. k_c is the total number of particles in contact with particle i. The m_i, v_i, I_i, and w_i are respectively the mass, velocity, moment

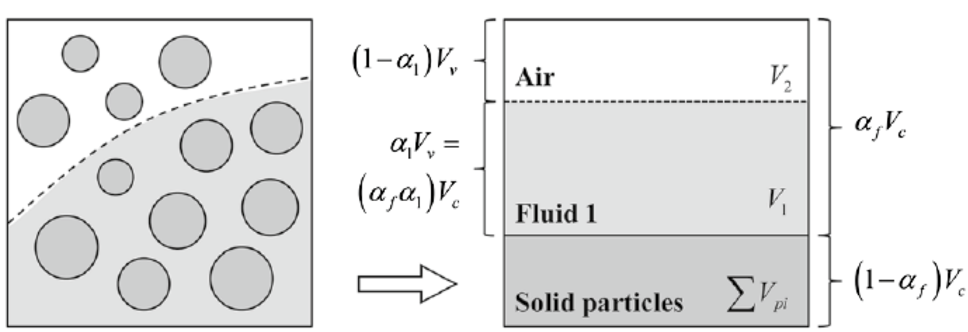

Fig. 1 Three-phase volume conservation

of inertia, and angular velocity of particles. The $M_{t,ij}$, $M_{r,ij}$ are the tangential torque and rolling torque between particles i and j, respectively. Hertz Mindlin model is adopted as the contact model, and its tangential and normal stiffnesses are related to Young's modulus, Poisson's ratio, and particle radius [22–25].

2.2 Continuum model of interstitial water

The locally averaged Navier–Stokes equation is used to describe the movement of interstitial water [26], and the VOF method is used to trace the free surface of the liquid. The Navier–Stokes equations for an incompressible viscous fluid are extended as

$$\frac{\partial(\varepsilon_f \rho_f)}{\partial t} + \nabla \cdot \left(\varepsilon_f \rho_f u_f\right) = 0 \tag{3}$$

$$\begin{aligned}&\frac{\partial(\rho_f \varepsilon_f u_f)}{\partial t} + \nabla \cdot (\rho_f \varepsilon_f u_f u_f) \\ &= \mu \nabla^2 u_f - \nabla p_{rgh} - g \cdot h \nabla \rho_f \\ &\quad + \sigma \kappa \nabla \alpha + F_{fp}^B\end{aligned} \tag{4}$$

where u_f is the velocity of fluid, ρ_f is the density of fluid, ε_f is the volume fraction of fluid, p_{rgh} is modified pressure by the coordinate vector, σ is the surface tension coefficient, μ is the dynamic viscosity of fluid, h is the coordinate vector, κ is the curvature of the free liquid surface, α_1 is the volume fraction of liquid in fluid, that is, saturation. F_{fp}^B is volumetric forces between fluid and particle.

The control equation of VOF method tracing the free surface of liquid is extended as

$$\frac{\partial(\alpha_1 \varepsilon_f)}{\partial t} + \nabla \cdot (\alpha_1 \varepsilon_f u_f) + \nabla \cdot (\alpha_1 (1 - \alpha_1) \varepsilon_f c |u_f| \frac{\nabla \alpha_1}{|\nabla \alpha_1|}) = 0 \tag{5}$$

where c is the compression factor. The CFD-DEM method calculates the volume of particles and averages the influence of particles on each mesh. When particles flow into or out of the fluid mesh, the volume fraction of the fluid ε_f in the mesh will change. In VOF method, In VOF method, the ε_f is V_v/V_c. The α_1 is V_1/V_v. When the mesh is filled with fluid, $\varepsilon_f = 1$; When the mesh is filled with liquid, $\varepsilon_f \cdot \alpha_1 = 1$. Figure 1 shows the conservation of the three-phase volume of gas–liquid-particles, where V_c is the mesh volume, V_v is the fluid volume.

The fluid-particle interaction forces mainly consist of all types of the forces acting on the individual particle by the fluid, such as drag force, pressure gradient force, virtual mass force, and Magnus force, etc. In this study, only the drag force and buoyancy are considered. The force of particles on fluid per unit volume[27] is

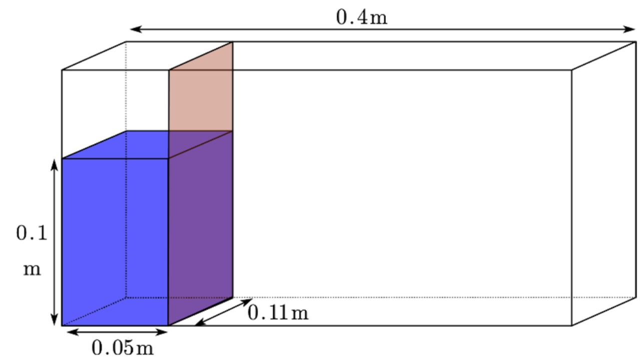

Fig. 2 Sketch of the simulation setup for the collapse of wet granular columns

$$F_{pf,i}^B = \frac{1}{\varepsilon_f V_{cell}} \sum f_{d,i} - \frac{1}{V_{cell}} \sum \left(\rho_f V_{p,i} g\right) \tag{6}$$

Accordingly, the acting force of the fluid on the particle phase is expressed as:

$$f_l = f_{fp,i}^B = \frac{1}{\varepsilon_f} f_{d,i} - \rho_f V_{p,i} g \tag{7}$$

where $f_{d,i}$ are forces between fluid and particle, V_{cell} is the volume of a fluid mesh, ε_f is the volume fraction of fluid, $V_{p,i}$ is the volume of particle i. $f_{d,i}$ is obtained from DiFelice traction formula:

$$f_{d,i} = 0.125 C_d \rho_f \pi d_p^2 \varepsilon_f^2 |u_f - v| (u_f - v) \varepsilon_f^{-\chi} \tag{8}$$

where,C_d is the drag coefficient, Re_p is the relative Reynolds number around the particle, χ is the correction coefficient for ε_f in dense particle system, $\mathbf{u}_f$ is translational velocity of fluid. C_d, etc. are obtained from the following empirical formula:

$$C_d = (0.63 + 4.8/\mathrm{Re}_p^{0.5})^2 \tag{9}$$

$$\mathrm{Re_p} = \rho_f d_p \varepsilon_f |u_f - v| / \mu \tag{10}$$

$$\chi = 3.7 - 0.65 \exp[-(1.5 - \log_{10} \mathrm{Re}_p)^2 / 2] \tag{11}$$

The calculated fluid-particle interaction force is updated to the particle motion equation.

2.3 Liquid-bridge model of interstitial water

The liquid bridge model is based on the discrete element method, and the capillary force of water is added to the interaction between particles. The model assumes that the particles are round and smooth, and the influence of gravity on the liquid bridge is ignored. The liquid bridge force is obtained by

Table 1 Simulation parameters of liquid-bridge model and CFD-DEM model

Properties	Numerical value
DEM	
Particle density	2510 kg/m^3
Particle radius	1/1.5/2 mm
Young's modulus	5×10^7 Pa
Poisson's ratio	0.23
Restitution Coefficient	0.2
Friction Coefficient	0.2\0.4\0.6\0.8
Time step	0.00001 s
Liquid-bridge	
Max Separation Distance Ratio	1.1
Min Separation Distance Ratio	1.01
Surface Tension	0.074 N/m
Fluid Viscosity	$0.00091 \text{ Pa}\cdot\text{s}$
Contact Angle	0.61
Surface Liquid Content Initial	0.0667/0.1333/0.2/0.2666
CFD	
Liquid density	1000 kg/m^3
Dynamic viscosity of liquid	$0.001 \text{ Pa}\cdot\text{s}$
Gas density	1.2 kg/m^3
Dynamic viscosity of gas	$0.0000148 \text{ Pa}\cdot\text{s}$
Time step	0.001 s
Model type	model B
Drag force	DiFeliceDrag; Archimedes
Saturation	30%/40%/…/100%
Coupling interval	100

approximating the shape and curvature of the liquid bridge. The capillary force expression of the liquid bridge [28]is:

$$f_l = \pi\gamma\sqrt{R_1R_2}[c + \exp\left(a\frac{D}{R_2} + b\right)] \tag{12}$$

where R_1, R_2 are radii of two particles respectively, D is the distance between the centers of two particles, θ is the contact angle, and γ is the liquid surface tension. The a, b, and c are respectively determined by the following formula:

$$a = -1.1\left(\frac{V}{R_2^3}\right)^{-0.53} \tag{13}$$

$$b = (-0.148\ln\left(\frac{V}{R_2^3}\right) - 0.96)\theta^2 - 0.0082\ln\left(\frac{V}{R_2^3}\right) + 0.48 \tag{14}$$

$$c = 0.0018\ln\left(\frac{V}{R_2^3}\right) + 0.078 \tag{15}$$

$$V = \varphi\cdot V_p \tag{16}$$

$$\alpha = \frac{1-\varepsilon_f}{\varepsilon_f}\cdot\varphi \tag{17}$$

where V is the volume of the liquid bridge, α is the saturation, V_p is the volume of total particles, ε_f is porosity, φ is the volume fraction of liquid volume to particle volume

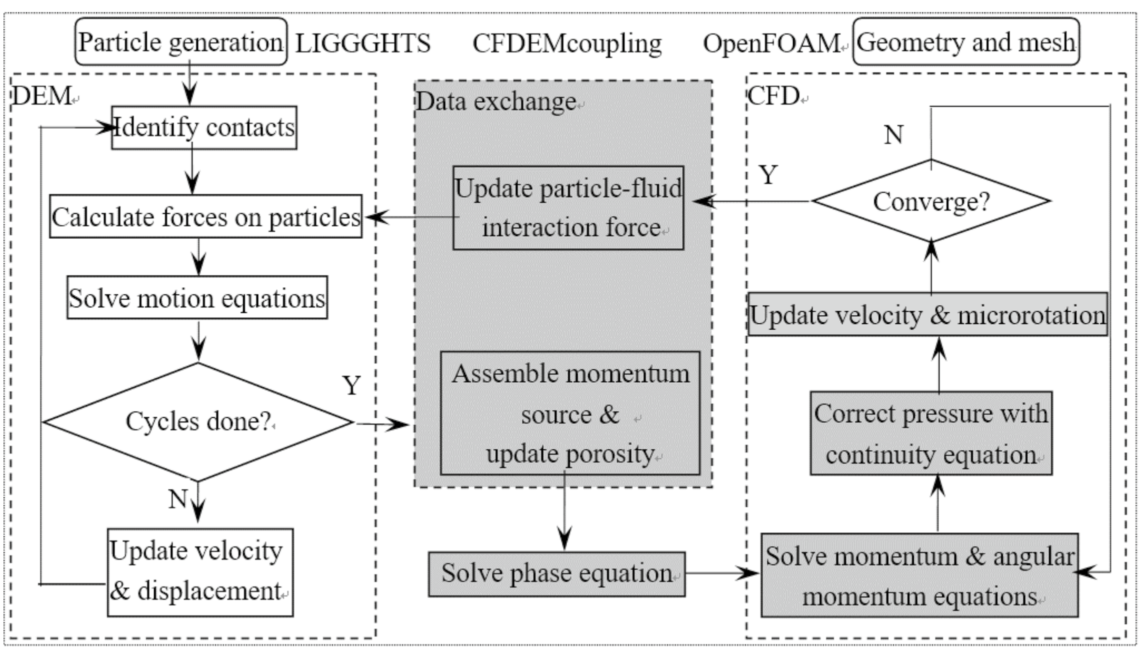

Fig. 3 Diagram of fluid-particle coupling calculation

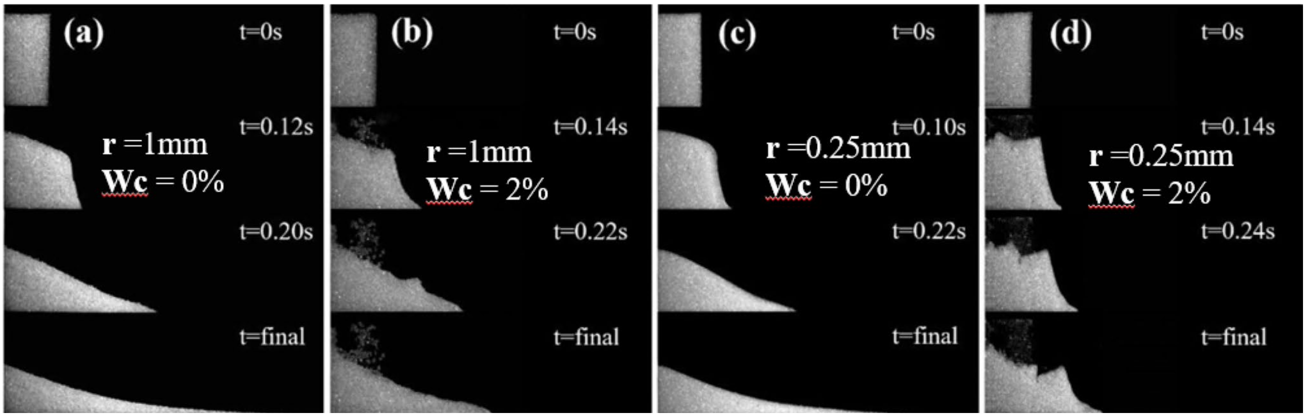

Fig.4 Experimental photos of continuous collapsed and block collapsed [10]

in initial conditions. In the liquid bridge model, capillary force is added to the particle motion equation, i.e., in Eq. (1), to simulate the effect of interstitial water on the particle's mechanical behavior. In the liquid bridge model, the liquid bridge force is mainly determined by the volume of liquid bridge, liquid surface tension, and particle radius.

3 Simulation setup and calculation process

3.1 Simulation setup

Figure 2 shows the setup of the simulation for wet granular column collapse. The simulation was conducted in a long rectangular tank of 0.11 m in width and 0.2 m height. Firstly, the vertical baffle is used to isolate the particle accumulation area, and the particles are accumulated in the designated area. When the granular column height of accumulation reaches 0.1 m, the baffle is removed, and the granular column begins to collapse.

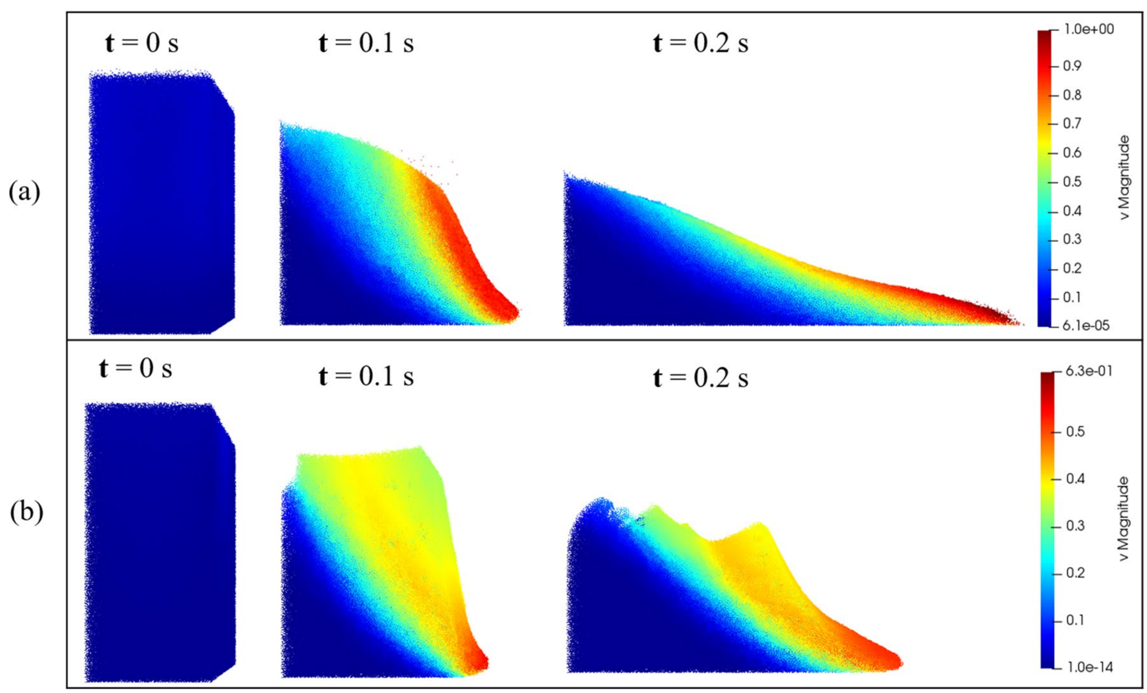

Fig.5 Simulation diagram of continuous collapsed and block collapsed: **a** Particle radius 0.5 mm, saturation 0%; **b** Particle radius 0.5 mm, saturation 10%

The simulation parameters are shown in Table 1, where the particle parameters are set with reference to sand, and the liquid parameters are set with reference to water. The total simulation time is 1.5 s. In the CFD-DEM model, saturation α_1 can be uniform given in the initial conditions. In the liquid bridge model, the saturation is given by φ in Eq. (17).

3.2 Calculation process

In this study, CFD-DEM calculation is based on open-source software OpenFOAM and LIGGHTS, as shown in Fig. 3. First, the DEM calculation takes several steps to transfer particle information, such as position coordinates and velocity, to the fluid phase. After the porosity is updated and the fluid calculation converges, the force exerted by the fluid on the particles is transferred to the particle phase, and the stress state of particles is updated. In this way, a coupling calculation is completed, and so on, until the maximum number of solving steps is reached.

The calculation process of the liquid bridge model is the same as the DEM process. Search the surrounding particles according to the particle number, calculate the size of the contact force and the liquid bridge force, and update the motion equation of the particles. After the particles move for a time step, start the next search calculation until the total simulation time is reached.

4 Verification and analysis

4.1 Verification

This section verifies the simulation of the CFD-DEM model and the liquid bridge model and compares the two models.

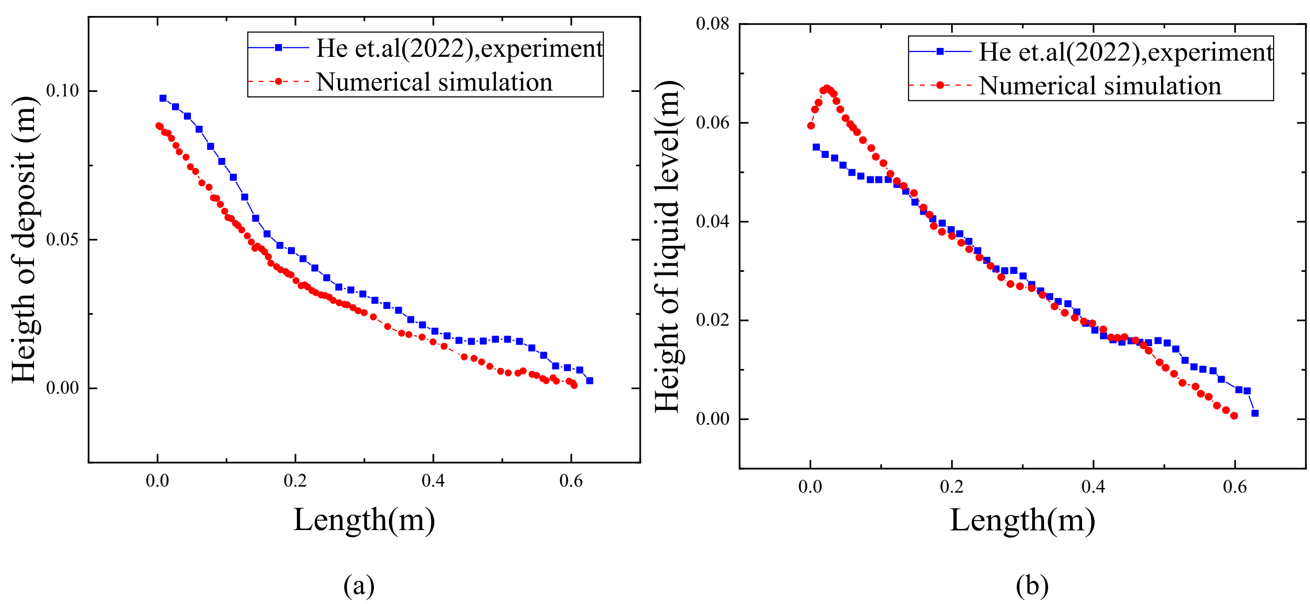

Fig.6 CFD-DEM model comparison with and experiment [6] **a** final deposit shape **b** final liquid level shape

Fig.7 Saturation contour of wet granular column

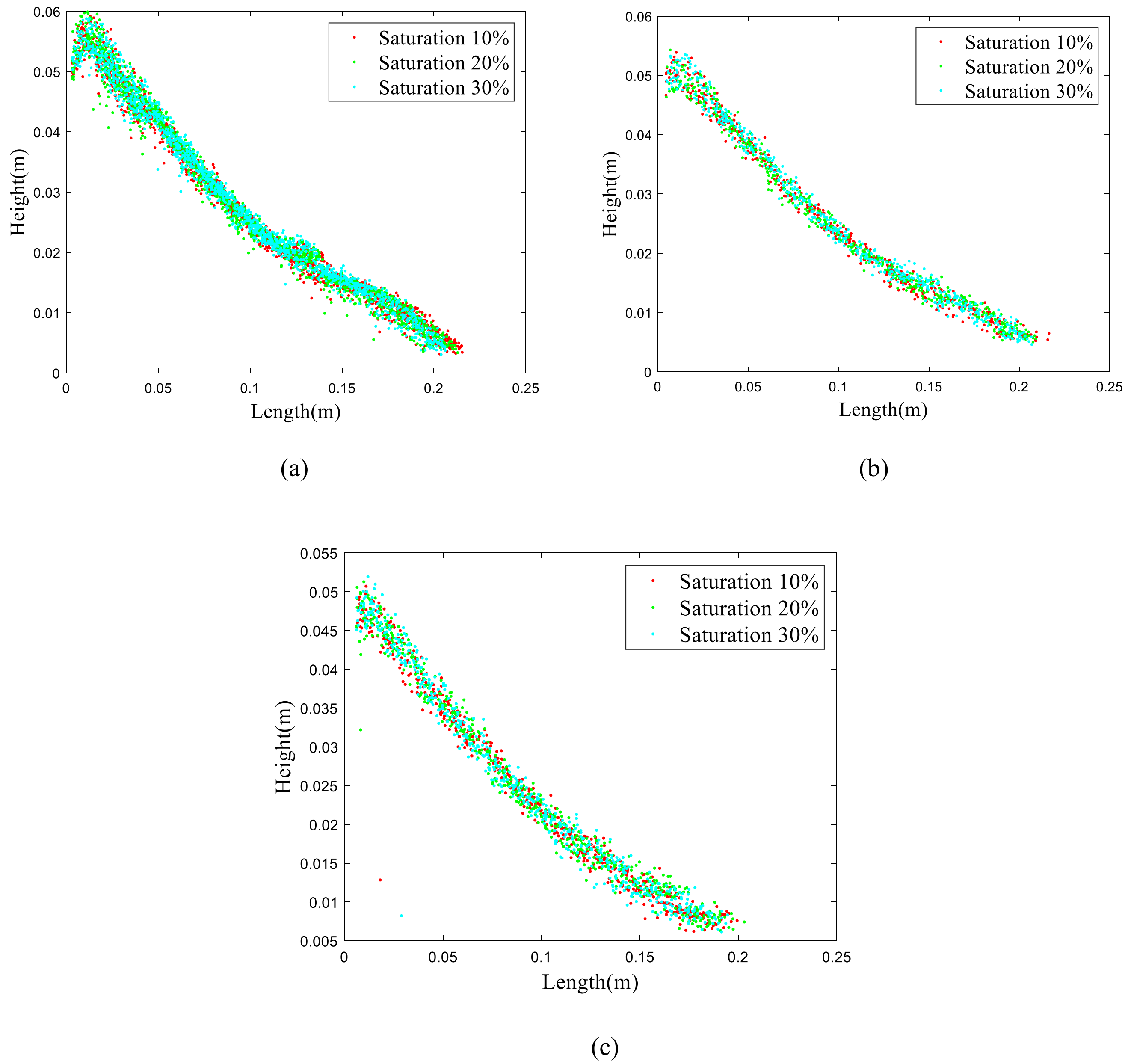

Fig.8 The final deposit shape of liquid-bridge model with different radius **a** radius 1 mm**b** radius 1.5 mm **c** radius 2 mm

4.1.1 Verification of liquid bridge model

Li et al. [10] divided the collapse morphology of the granular column into three types, continuous collapsed (c–c), block collapsed (b–c), and non-collapse. Figure 4 shows the experimental photos of continuous collapsed and block collapsed. (a) and (c) are continuous collapsed, (b) and (d) are block collapsed, and Wc is water content, that is, water mass/particle mass. The saturation corresponding to water content 2% is about 7.5%.

In the case of dry particles with particle radii of 1 mm and 0.25 mm, respectively, the height profile of the deposit pile is approximately a monotonous, continuous, smooth contour and without bulge, as shown in Fig. 4 a, c. However, when the water content is 2% and the particle radius is 1 mm and 0.25 mm, respectively, the height profile of the deposit pile is not smooth and step-like. This is because of the cohesive effect between the particles, some particles locally agglomerate together, accompanied by local sliding and tumbling, as shown in Fig. 4b, d. Figure 5 a, b shows the flow state of continuous collapsed and block collapsed simulated by liquid-bridge model, which is consistent with the experimental results of Li et al. [10]

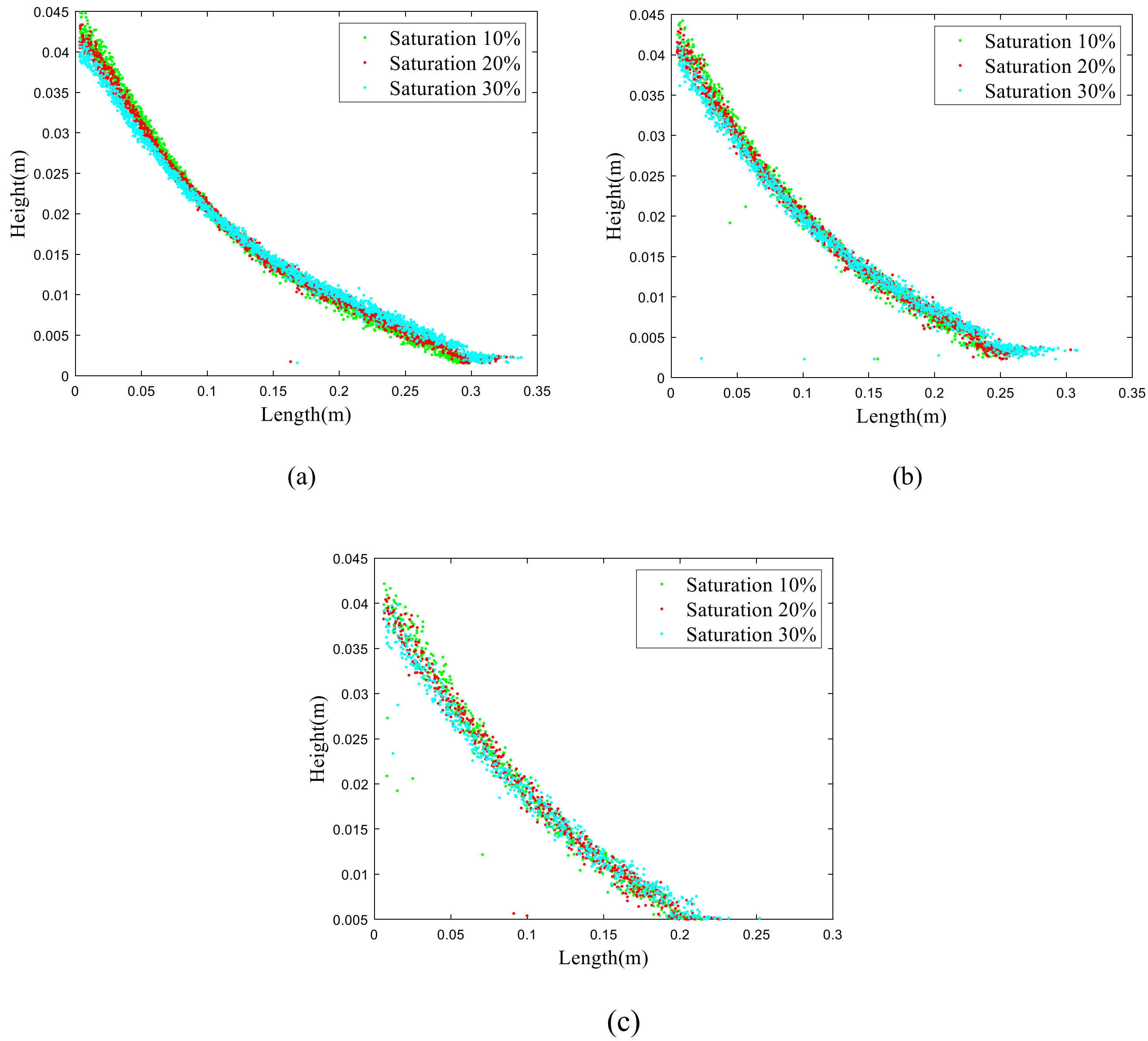

Fig.9 The final deposit shape of CFD-DEM model with different radius **a** radius 1 mm**b** radius 1.5 mm **c** radius 2 mm

4.1.2 Verification of CFD-DEM model

Referring to the experiment of He et al. [6], CFD-DEM model was used to simulate the collapse of a wet granular column under 100% saturation. The simulation process is the same as that in Sect. 3, and the size of the rectangular tank has changed. The length, width, and height of the granular column are 13 cm, 20 cm, and 16 cm, respectively, and the particle radius is 3.01 mm. Other particle parameters and fluid parameters remain unchanged. The final deposit shape and final liquid level shape of the granular column are consistent with the experimental data, which verifies the CFD-DEM model, as shown in Fig. 6. Figure 7 shows the saturation contour during the collapse of wet granular column.

4.1.3 Comparison between CFD-DEM model and liquid bridge model

The CFD-DEM model is compared with the liquid bridge model in the saturation range of 10–30%. Figure 8a, b, and c show the morphology of the liquid bridge model at

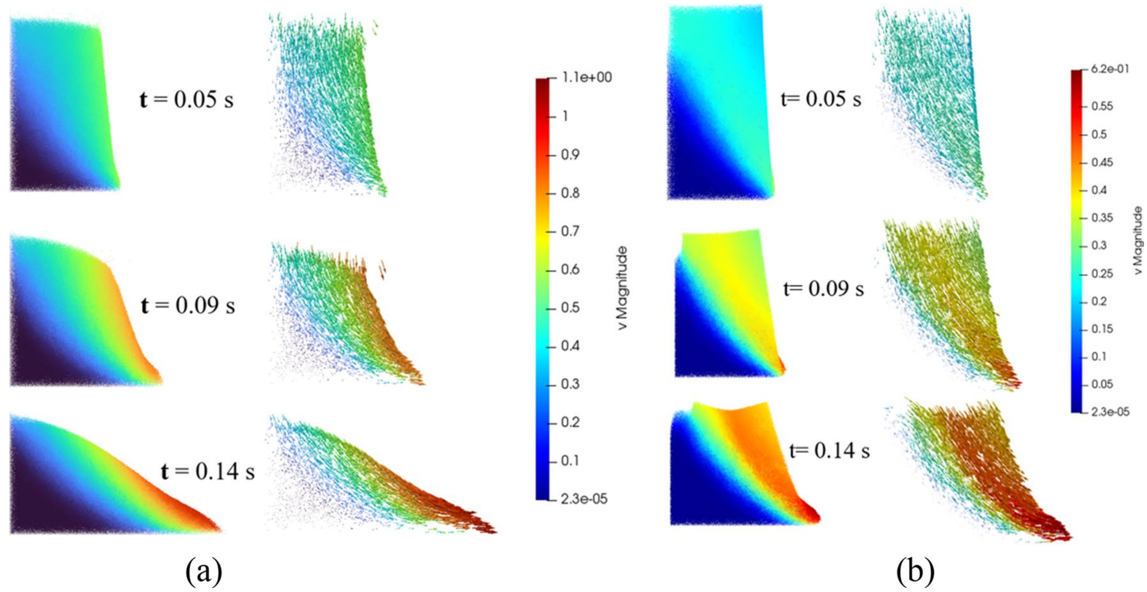

Fig10 Vector graphics of continuous collapsed and block collapsed **a** Dry particles with radius of 0.5 mm **b** Wet particles with radius of 0.5 mm and saturation of 10%

different saturations of 1 mm, 1.5 mm, and 2 mm particle sizes, respectively, and Fig. 9a, b and c show the simulation results of the CFD-DEM model. As shown in the figure, different conclusions have been drawn from the two models. In the liquid bridge model, the variation of saturation has little impact on the final deposit shape, which is consistent with the experiment of Li et al. [10]. In the CFD-DEM model, the influence of saturation on the final deposit shape is more obvious, which will be further elaborated on in the analysis later.

CFD-DEM model can not simulate different flow patterns because the force of interstitial water on particles is different

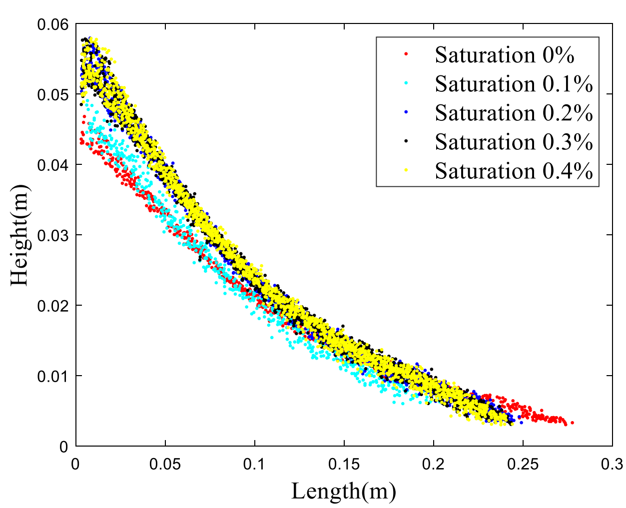

Fig.11 The final deposit shape within saturation from 0 to 0.4% (radius 1 mm)

under different saturation. Fournier et al. [29], Rossetti et al. [30] classified the morphology into four types according to the different existing forms of interstitial water, namely pendular state, funicular state, capillary state, and slurry state. In the range of 0–30% saturation, the interstitial water is the pendular state; in saturation 30–70%, it is the funicular state; in 70–100%, it is the capillary state; and in supersaturated, it is the slurry state. In the pendulum state, the liquid bridge is formed at the contact point of particles; in the funicular state, part of the particle interval is filled with liquid; in the capillary state, almost all the particles interval is filled with liquid; in the slurry state, the liquid pressure is greater than the air pressure. Therefore, liquid-bridge model is adopted for granular materials within saturation below 30%, and CFD-DEM model is adopted for other saturation in this study.

4.2 Analysis of numerical simulation

4.2.1 Dynamic analysis and analysis of final deposit shape within saturation range from 0 to 30%

Figure 10 shows the velocity contour of block collapsed and continuous collapsed, where the particle radius in block collapse is 0.5 mm, and the saturation is 10%; in continuous collapse, the particle radius is 0.5 mm, and the saturation is 0%. In Fig. 10, the color variation indicates the particle velocity, the direction of the arrow indicates the motion direction, and the length of the arrow indicates the motion velocity. In (a) (b), the left side shows the complete collapse morphology, and the right side only shows the moving part. The process

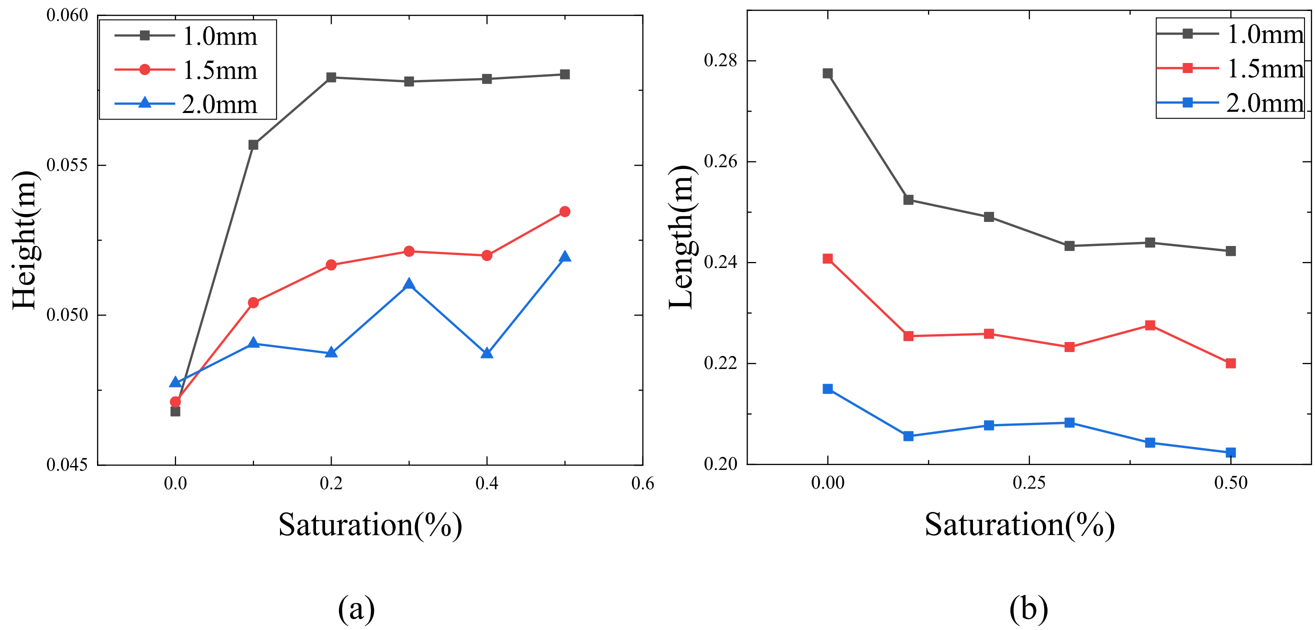

Fig.12 Variation of final deposit height and length within saturation from 0.1 to 0.5% **a** height **b** length

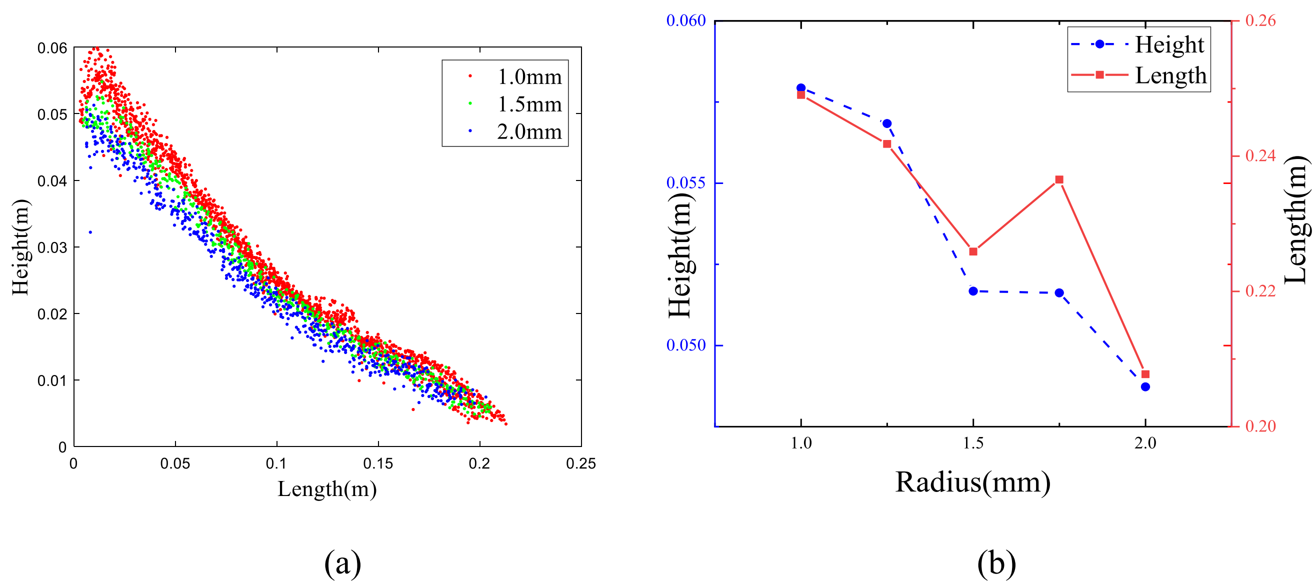

Fig.13 Variation of final deposit shape with particle radius (saturation 20%) **a** shape diagram **b** variation diagram

of particle column collapse is that particles near the outer boundary slide and accumulate along the boundary under the influence of gravity. In the continuous collapsed state, the particles at the boundary collapse first. The particle velocity closer to the boundary is faster, and the velocity variation is also continuous. In the block collapsed, the velocity variation is not continuous. There are different velocity layers. The velocity in the middle area is fast, and the velocity on both sides is slow, resulting in a velocity difference. This is because the particles in the flow process are agglomerated due to the effect of interstitial water, and the flow velocity is no longer continuous. When the agglomeration area is large enough, the collapse will not occur (Fig. 10).

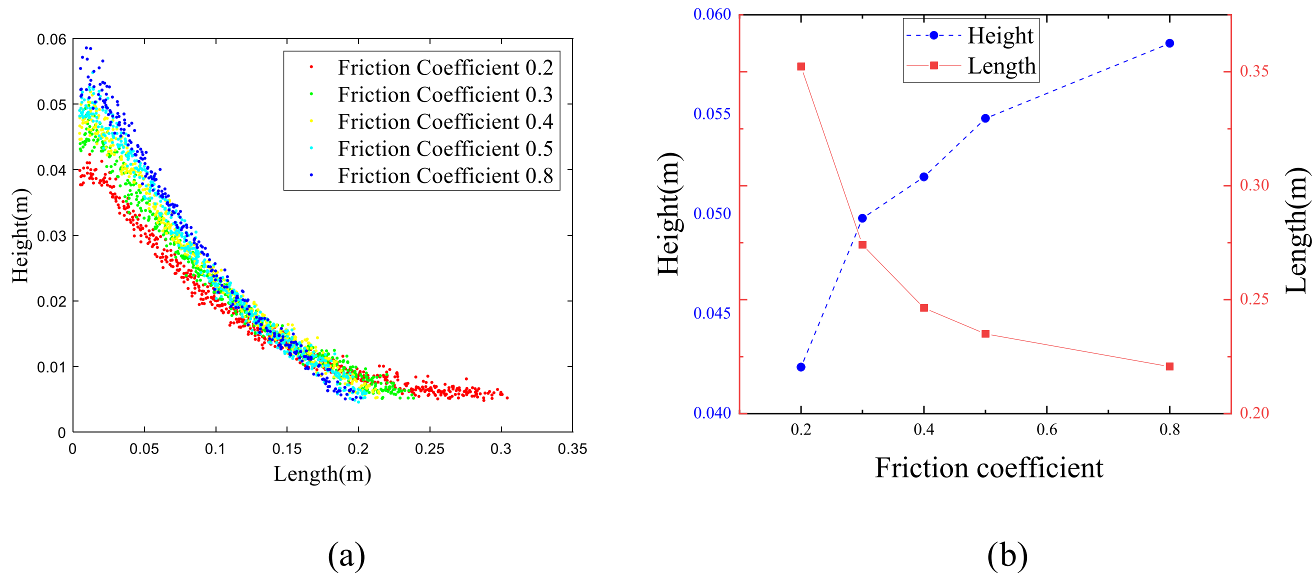

Fig.14 Variation of final deposit shape with friction coefficient (saturation 20%) **a** shape diagram **b** variation diagram

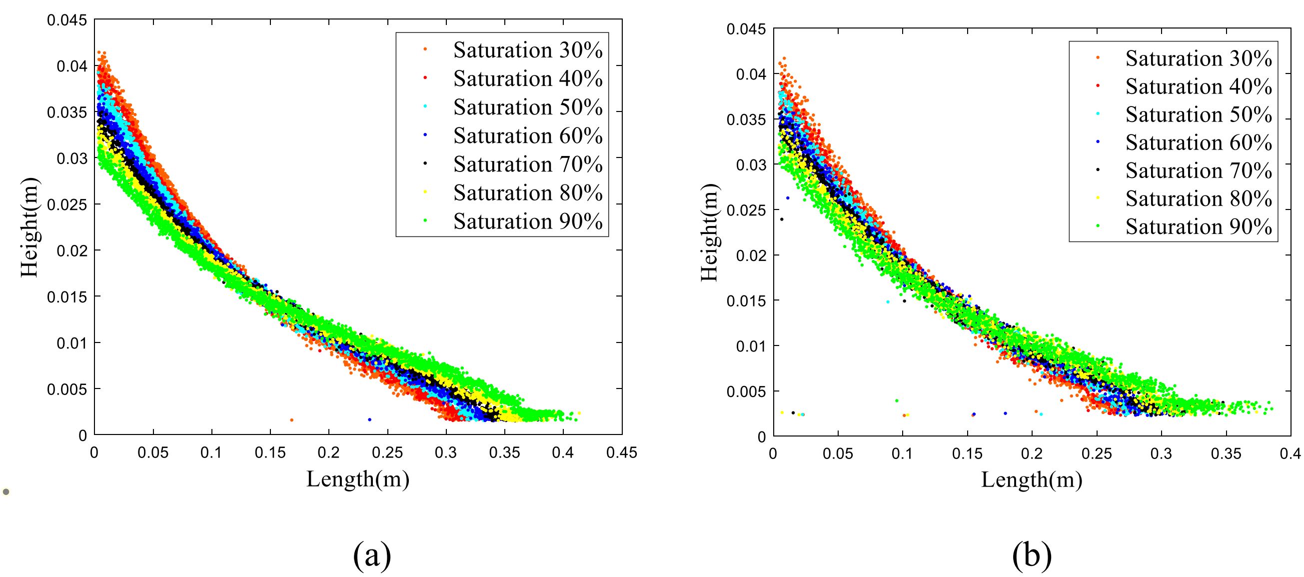

Fig15 The final deposit shape varied from saturation to 30–90% **a** radius 1 mm **b** radius 1.5 mm

Through the variation of the boundary shape of the final deposit, the influence of different saturation, particle size, and friction coefficient on the shape of the final deposit was studied. Figure 11 shows the final deposit shape of a wet particle column with radius of 1 mm and saturation of 0.1–0.4%. In this range, saturation has a significant impact on the final deposit shape. Figure 12a shows the deposit height increase with the increase of saturation, and Fig. 12b shows the deposit length decrease with the increase of saturation. This study also analyzes the influence of particle radius. Figure 13 shows the variation of the final deposit height and length of the particle column with particle radius under 20% saturation. In the saturation range of 10–30%, the deposit height and deposit length decrease with the increase of radius. In addition, the influence of the friction coefficient is studied. As shown in formula (12), (13), (14),

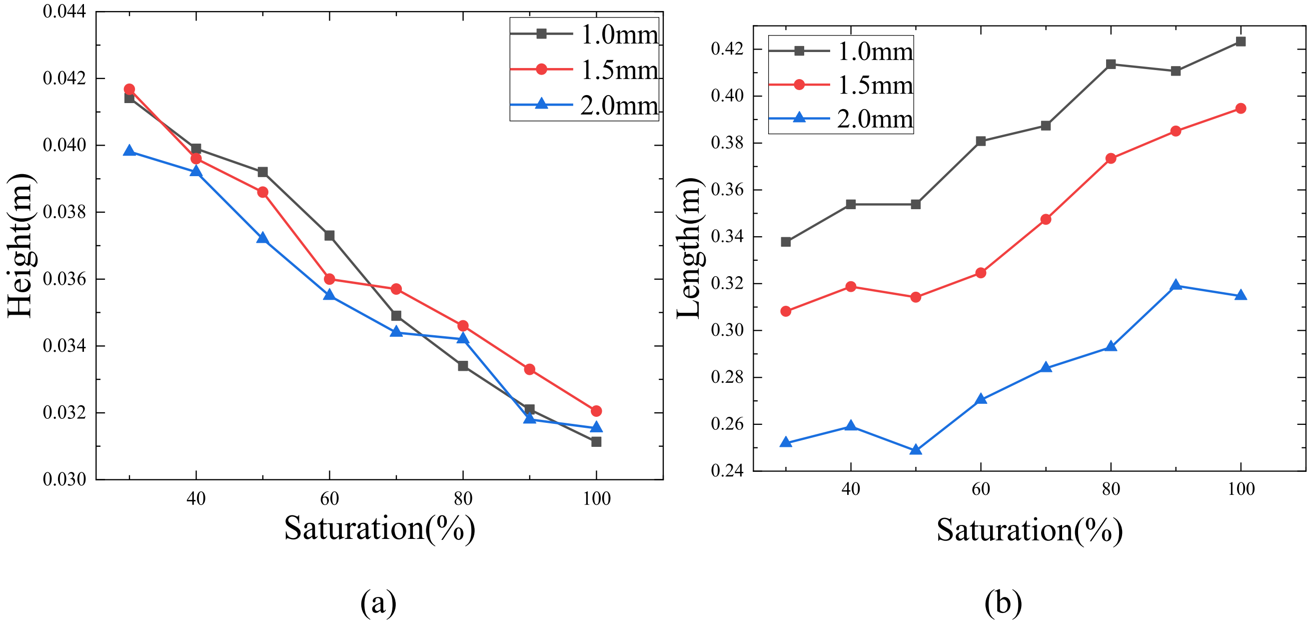

Fig.16 Variation of final deposit height and length with saturation **a** height **b** length

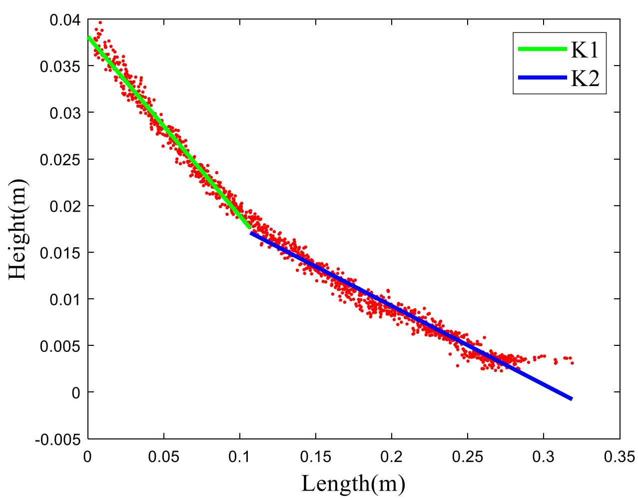

Fig.17 Final deposit boundary fitting diagram

and (15), the size of the liquid bridge force is related to the particle radius, and the main driving force of the collapse of the particle column is the gravity of the particle, so the mechanism for this phenomenon may be related to the change of the ratio between the liquid bridge force and the gravity of the particle with particle radius. Noted that this phenomenon was also observed in other experiments and numerical simulations [6]. However, the mechanism needs to be further investigated. As shown in Fig. 14, the deposit height increases with the increase of friction coefficient, and the length decreases with the increase of friction coefficient. In the subsequent simulation, the friction coefficient is 0.5.

4.2.2 The analysis of final deposit shape within saturation range from 30 to 100%

Figure 15a and b show the final deposit shape of a granular column within saturation from 30 to 90%, and the variation of saturation within this range has a significant impact on the final deposit shape. As shown in Fig. 16a, b, when the saturation is 30–90%, the final deposit height decreases with the increase of saturation, and the final deposit length increases with the increase of saturation. The bilinear model is used to fit the final deposit boundary shape. The point where the product of the fitting correlation coefficient of the two straight lines reaches the maximum is the boundary point of the two lines. Figure 17 is the fitting diagram. After obtaining the fitting line, we analyzed the slope variation of the two fitting lines. The slope of the fitting line close to the upper boundary is K1, and that close to the lower boundary is K2. As shown in Fig. 18a, b, the slopes of the two straight lines decrease with the increase of saturation in the range of 30–100%.

4.2.3 Fluidity analysis based on mass center motion

Analyze the motion distance of the mass center, where Hmc represents the drop height of the mass center, Lmc represents the horizontal run-out distance of the mass center, and arctan (Hmc/Lmc) represents the angle of the mass center motion. Figure 19 shows the motion distance of the mass center with different saturation and different radius in the CFD-DEM model. Different lines represent different radii,

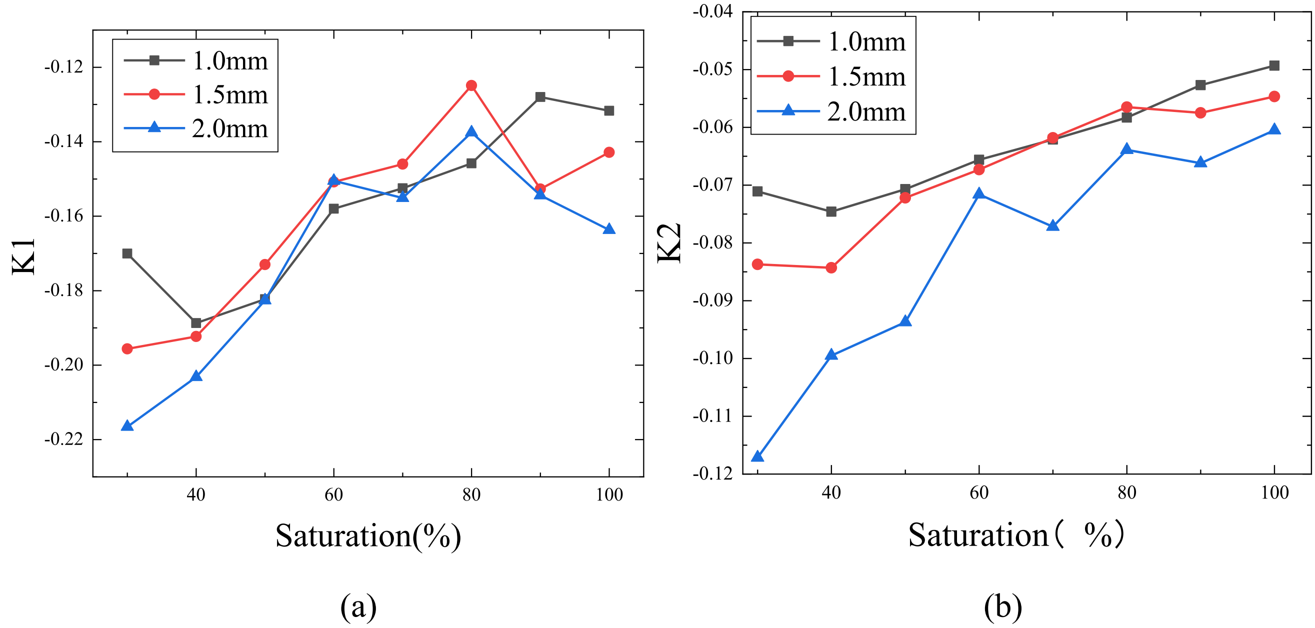

Fig.18 Variation of the slope of fitting line of final deposit with saturation

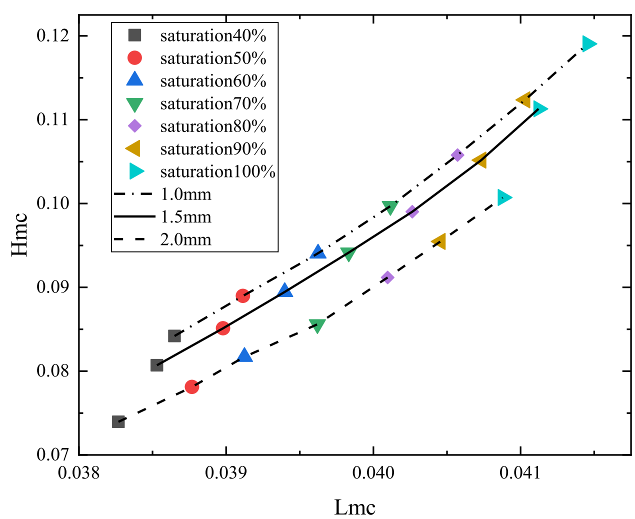

Fig.19 The diagram of mass center motion

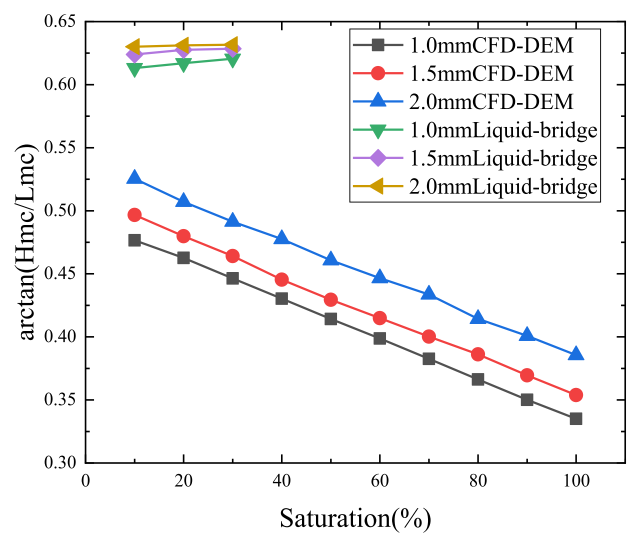

Fig.20 The variation of the angle of the mass center motion

and different colors and shapes represent different saturations. The motion distance of the mass center of granular materials increases with the increase of the drop height and horizontal run-out distance of mass center, and accordingly, the fluidity is enhanced. In Fig. 19, an increase of saturation led to a gradual increase of the drop height of mass center and horizontal run-out distance of mass center. A decrease in radius led to a gradual increase of Hmc and Lmc. Therefore, the fluidity of granular materials increases with the increase of saturation and decreases with the increase of particle radius in the range of 40–100% saturation. Compared with Fig. 16, the influence of saturation and radius is consistent with that of Fig. 19, but the final deposit height does not change significantly with the radius, while the drop height of mass center varies greatly. This is because the motion distance of the mass center considers the motion of the particle

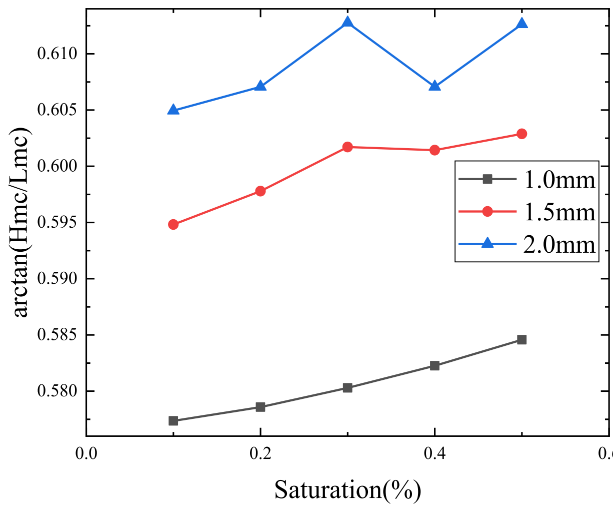

Fig.21 The variation of the angle of the mass center motion in saturation0.1–0.5%

globally, ignoring the influence of accidental factors such as the accumulation mode.

Figure 20 shows the variation of the angle of the mass center motion with saturation and compares the liquid bridge model with the CFD-DEM model. When the variation of the drop height of the mass center is inconsistent with the horizontal run-out distance of the mass center, the angle of the mass center motion can reflect the contribution of Hmc to Lmc. In the collapse of the granular column, the gravitational potential energy makes the main contribution. So with the decrease of the angle of the mass center motion, the transformed gravitational potential energy increases, and the fluidity of the particle material increase. In Fig. 20, the fluidity of granular materials in CFD-DEM model increases with the increase of saturation, while the fluidity of the liquid bridge model does not vary significantly in the saturation range of 10–30%. The analysis of the angle of the mass center motion shows the comparison of the two models more clearly. Reference Li et al. [10], the liquid bridge model is applicable to the pendular state with saturation lower than 30%, while the CFD-DEM model is applicable to the state with saturation of more than 30%.Fig. 21 shows that the fluidity of granular materials decreases with the saturation, in saturation from 0.1 to 0.5%.

5 Conclusion

In this study, saturation is used to describe the variation of water content, and the wet particle column within saturation from 0 to 100% is numerically simulated. The liquid bridge discrete element model and CFD-DEM model are verified by comparison with the experiment, respectively. After comparing the two models, the liquid-bridge model is adopted at 0% to 30%, and the CFD-DEM model is adopted at 30% to 100%. The following conclusions are as follows:Q4

(1) The influence of saturation on deposit shape is investigated; in the saturation range of 0.1–0.5%, the deposit height increases with the increase of saturation, and the length decreases with the increase of saturation. In the range of 0.5–30%, Saturation has little effect on the final deposit shape. In the range of 30–100%, the deposit height decreases with the increase of saturation, and the length increases with the increase of saturation. The bilinear model is used to fit the deposit boundary, and the slope of the fitted two straight lines decreases with the increase of saturation in the saturation 30–100%.

(2) The fluidity of the granular column collapsed was studied by the mass center motion and angle of mass center motion. In the range of 0.1–0.5% the fluidity decrease with saturation; in the range of 0.5–30% saturation, saturation has little effect on fluidity of granular materials, but in the range of 30–100% saturation, the fluidity of granular materials increases with the increase of saturation.

(3) The deposit height increases with the increase of friction coefficient, and the deposit length decreases with the increase of friction coefficient. And the fluidity of granular materials decreases with the increase of particle radius.

Acknowledgements This study was supported by the National Natural Science Foundation of China (No. 12172263).

Declarations

Conflict of interest The authors declare that they have no conflict of interest.

References

1. Patrice, P., Hugo, S.C.: Tensile strength of wet granular materials. Powder Tehnology pp. 83–93 (1997)
2. Jarray, A., Magnanimo, V., Luding, S.: Wet granular flow control through liquid induced cohesion. Powder Technol. **341**, 126–139 (2019)
3. Wang, F.W., et al.: Mechanism for the rapid motion of the Qianjiangping landslide during reactivation by the first impoundment of the Three Gorges Dam reservoir China. Landslides **5**(4), 379–386 (2008)
4. Zhang, X., et al.: Quasi-static collapse of two-dimensional granular columns: insight from continuum modelling. Granul. Matter **18**(3) (2016)
5. Topin, V., et al.: Collapse dynamics and runout of dense granular materials in a fluid. Phys. Rev. Lett. **109**(18), 188001 (2012)

6. He, K., Shi, H., Yu, X.P.: Effects of interstitial water on collapses of partially immersed granular columns. Phys. Fluids **34**(2) (2022)
7. Santomaso, A.C., Volpato, S., Gabrieli, F.: Collapse and runout of granular columns in pendular state. Phys. Fluids **30**(6) (2018)
8. Wu, Y.S., Wang, D.M., Li, P.S.: The collapse of a granular column onto an erodible bed: dynamics and morphology scaling. Granul. Matter **23**(2) (2021)
9. Berzi, D., Bossi, F.C., Larcan, E.: Collapse of granular-liquid mixtures over rigid, inclined beds. Phys. Rev. E Stat. Nonlinear Soft Matter Phys. **85**(5 Pt 1), 051308 (2012)
10. Li, P.S., et al.: Experimental study on the collapse of wet granular column in the pendular state. Powder Technol. **393**, 357–367 (2021)
11. Yuan, C., et al.: Numerical simulation of wetting-induced collapse in partially saturated granular soils. Granul. Matter. **21**(3) (2019)
12. Tamura, K., et al.: Validation study on a toroidal approximation-based capillary force model in the discrete element method simulation. Phys. Fluids **34**(2) (2022)
13. El-Emam, M.A., et al.: Theories and applications of CFD–DEM coupling approach for granular flow: a review. Arch. Comput. Methods Eng. **28**(7), 4979–5020 (2021)
14. Golshan, S., et al.: Review and implementation of CFD-DEM applied to chemical process systems. Chem. Eng. Sci. **221** (2020).
15. Zhao, J., Shan, T.: Coupled CFD–DEM simulation of fluid–particle interaction in geomechanics. Powder Technol. **239**, 248–258 (2013)
16. Tanaka, T., Kawaguchi, T., Tsuji, Y.: Discrete particle simulation of flow patterns in two-dimensional gas fluidized beds. Int. J. Modern Phys. B **07**(09n10), 1889–1898 (2012)
17. Li, X., Chu, X., Sheng, D.C.: A saturated discrete particle model and characteristic-based SPH method in granular materials. Int. J. Numer. Methods Eng. **72**(7), 858–882 (2007)
18. Jing, L., et al.: Extended CFD-DEM for free-surface flow with multi-size granules. Int. J. Numer. Anal. Methods Geomech. **40**(1), 62–79 (2016)
19. Wang, L., Chu, X.: An extended CFD-DEM model based on micropolar fluid and its application in geological engineering. Comput. Geotech. **154** (2023)
20. Yu, F., Su, L.: Experimental investigation of mobility and deposition characteristics of dry granular flow. Landslides **18**(5), 1875–1887 (2021)
21. Cundall, P.A., Strack, O.D.L.: A discrete numerical model for granular assemblies. Geotechnique **29**(1), 47–65 (1979)
22. Hertz, H.: On the contact of elastic solids. Crelle's J. **92**, 156–171 (1880)
23. Tsuji, Y., Tanaka, T., Ishida, T.: Lagrangian numerical simulation of plug flow of cohesionless particles in a horizontal pipe. Powder Technol. **71**(3), 239–250 (1992)
24. Di Renzo, A., Di Maio, F.P.: An improved integral non-linear model for the contact of particles in distinct element simulations. Chem. Eng. Sci. **60**(5), 1303–1312 (2005)
25. Mindlin, R.D.: Compliance of elastic bodies in contact. J. Appl. Mech. **16**(3), 259–268 (1949)
26. Sun, X.S., Sakai, M.: Three-dimensional simulation of gas–solid–liquid flows using the DEM–VOF method. Chem. Eng. Sci. **134**, 531–548 (2015)
27. Zhou, Z.Y., et al.: Discrete particle simulation of particle–fluid flow: model formulations and their applicability. J. Fluid Mech. **661**, 482–510 (2010)
28. Soulié, F., et al.: Influence of liquid bridges on the mechanical behaviour of polydisperse granular materials. Int. J. Numer. Anal. Methods Geomech. **30**(3), 213–228 (2006)
29. Fournier, Z., et al.: Mechanical properties of wet granular materials. J. Phys. Condens. Matter **17**(9), S477–S502 (2005)
30. Rossetti, D., Simons, S.J.R.: A microscale investigation of liquid bridges in the spherical agglomeration process. Powder Technol. **130**(1–3), 49–55 (2003)